Chinese Journal of Chemical Engineering 25 (2017) 211–215

Contents lists available at ScienceDirect

Chinese Journal of Chemical Engineering

journal homepage: www.elsevier.com/locate/CJChE

Chemical Engineering Thermodynamics

Effects of temperature and phosphoric acid addition on the solubility of iron phosphate dihydrate in aqueous solutions☆

Tongbao Zhang, Yangcheng Lu *, Guangsheng Luo

State Key Laboratory of Chemical Engineering, Department of Chemical Engineering, Tsinghua University, Beijing 100084, China

ARTICLE INFO

Article history:
Received 30 March 2016
Accepted 28 June 2016
Available online 2 July 2016

Keywords:
Iron phosphate
Solubility
Aqueous solution
Phosphoric acid
Temperature

ABSTRACT

As important controlling factors for the synthesis of iron phosphate materials by liquid-phase precipitation, the solubilities of iron phosphate dihydrate were systematically measured at H_3PO_4 concentrations from 1.13 wt% to 10.7 wt%, temperature from 298.15 to 363.15 K, and atmosphere pressure in this work. The solubility was found to increase 5 orders of magnitude or more with increasing the concentration of phosphoric acid, and decrease 1 to 2 orders of magnitude with increasing the equilibrium temperature. The phosphoric acid addition and temperature were found to affect the solubility of iron phosphate dihydrate by the formation or dissociation of coordination species, which could further accelerate the phase transformation from the amorphous iron phosphate dihydrate to orthorhombic iron phosphate dehydrate by dissolution–recrystallization mechanism. The high dependences of the solubility of iron phosphate materials on H_3PO_4 concentration and temperature were also well predicted by calibration equations, which are meaningful for quantitatively understanding the precipitation process and sequential crystalline structure transformation and pursuing a rational strategy for synthesizing specific iron phosphate materials.

1. Introduction

Interest in iron phosphate compounds has always been intensive due to their impressive performance and wide application in the fields of battery [1–2], catalysis [3–5], wastewater purification [6,7], ferroelectrics [8], and *etc.* [9]. It has been well recognized that the manipulation of the structure and size of iron phosphate materials is of great importance for achieving various and competitive functions [10–12]. For examples, as cathode materials for lithium/sodium ion batteries, iron phosphates with amorphous or orthorhombic heterosite structure were found to exhibit much better electrochemical performance due to the existence of plenty of migration routes for carrier ions [13–15]. Although α-Quartz iron phosphate is inert in electrochemical activity, it shows high performance to catalyze the gas-phase selective oxidation of benzene to phenol [16], in which the tetrahedral-coordinated Fe is the active center. As for enhancing the electrochemical performance or the catalytic activity, a choice is to facilitate both electron and carrier ions migration or expose more active sites by reducing the size of iron phosphate materials mentioned above.

The synthesis of iron phosphate compounds commonly starts from versatile precipitation reactions between dissolved iron (III) and phosphate ions in aqueous solution [17–23]. The reaction conditions, especially in terms of temperature and pH, directly determine the reactants participating in the fast precipitation process. In following, the growth process of the as-prepared precipitates affords products with diversity in size, morphology and crystalline structure [6,24]. The solubilities of iron phosphate materials are important controlling factors throughout the conversion process. Chang and Jackson firstly determined the solubility of strengite ($FePO_4 \cdot 2H_2O$) in water at room temperature after 8 to 21 days equilibrium experiments [25]. Assuming that $FePO_4 \cdot 2H_2O$ dissociates into Fe^{3+}, $H_2PO_4^-$ and OH^-, the calculated solubility product (K_{sp}) of strengite was between $10^{-33.5}$ and 10^{-35}. According to the heat capacities at temperatures between 8 and 310 K and the heat of formation at 298 K, Egan *et al.* obtained similar value ($10^{-34.56}$) by thermodynamic calculation [26]. The measurements on strengite solubility in dilute H_3PO_4 by Nriagu *et al.* [27] also confirmed the scale of K_{sp} ($10^{-34.88}$). Besides, Dean assumed that the amorphous iron phosphate ($FePO_4 \cdot 2H_2O$) dissociates into Fe^{3+}, PO_4^{3-} and H_2O in water, and reported K_{sp} of 9.92×10^{-29} at 298 K [28].

However, there exist complex dissociations and complexations in the aqueous solution of iron phosphate materials, and the calculation of solubility from K_{sp} is difficult. On the other hand, considering versatile iron phosphate materials and broad pH/temperature window for synthesis, the measurements on their solubilities are still scarce. In this work, we selected amorphous iron phosphate dihydrate (the direct product of precipitation) as solute, phosphoric acid as a pH regulator with foreign ions free, and systematically investigate the effects of

☆ Supported by the National Natural Science Foundation of China (21176136, 21422603) and the National Basic Research Program of China (2007CB714302).
* Corresponding author. Tel.: +86 10 62773017; Fax: +86 10 62770304.
E-mail address: luyc@tsinghua.edu.cn (Y. Lu).

http://dx.doi.org/10.1016/j.cjche.2016.06.009
1004-9541/

temperature and phosphoric acid addition on the solubility of iron phosphate dihydrate in aqueous solutions. The concentration of phosphoric acid and temperature varied from 1.13 wt% to 10.7 wt% and 298.15 to 363.15 K, respectively. The quantitative variation laws as well as fundamental data of solubilities were of great importance for understanding and designing iron phosphate materials synthesis processes.

2. Experimental Section

2.1. Chemicals

The iron (III) phosphate dihydrate ($FePO_4 \cdot 2H_2O$) was purchased from the Sigma-Aldrich. The orthophosphoric acid (H_3PO_4, aq. soln.) was purchased from Alfa Aesar. The hydrochloric acid (HCl, 36 wt%–38 wt%) was purchased from Beijing Chemical Works. All of the reagents were used as received without further purification. Ultrapure deionized water (18.2 MΩ) was used throughout the experiments for solution preparation and vessel cleaning.

2.2. Solution preparation

All the vessels used throughout the experiments were thoroughly cleansed. They were firstly washed by 1 $mol \cdot L^{-1}$HCl solution under sonication for 2 h to remove any possible impurities. Then the vessels were thoroughly rinsed by ultrapure deionized water and further sonicated for another 1 h. The water cleaning procedure was repeated for three times. Finally, they were dried at 105 °C in air overnight.

The H_3PO_4 solutions with various concentrations were prepared by diluting purchased 85% H_3PO_4 solution and stored in volumetric flasks. The exact concentrations of H_3PO_4, determined by an inductively coupled plasma-optical emission spectrometer, were listed in Table 1, in which the pH value and density measured at room temperature were also provided.

2.3. Equilibrium procedure

A typical equilibrium procedure was described as follows. Firstly, 50 ml of phosphoric acid solution was transferred to conical flask added with sufficient amount of $FePO_4 \cdot 2H_2O$ powders in advance. And then, the conical flask was sealed and placed in a thermostatic oven (DHG-9035A, HONGHUA) at temperature above 308.15 K, or in a thermostatic bath equipped with a refrigeration system (LSHZ-300, HAOCHENG) at temperature below 308.15 K. The temperature uncertainty for equilibrium was ±0.1 K. According to Chang's results [25], the equilibrium time was set as long as 30 days to approach the liquid–solid equilibrium, after which the supernatant was carefully drawn out by a single-use syringe. The syringe nozzle was equipped with a 0.22 μm filter head to remove any possible solid and get clear liquid samples for solubility measurement. The residual solid was isolated by suction filtration, washed by water, and dried at 105 °C in air overnight for crystalline structure characterization.

2.4. Analysis and characterization

The iron and phosphorus contents in liquid samples were analyzed by an inductively coupled plasma-optical emission spectrometer (ICP-OES, iCAP6300, ThermoFisher) or an inductively coupled plasma-mass spectrometer (ICP-MS, iCAPQ, ThermoFisher). The limit of detection of ICP-OES for iron is $10^{-8}\ g \cdot g^{-1}$. The power of the plasma was 1150 W. Peristaltic pump rotation speed was $100\ r \cdot min^{-1}$. The limit of detection of ICP-MS for iron is $10^{-12}\ g \cdot g^{-1}$. The power of the plasma was 1548 W. Argon gas in high-purity (99.9999%) was used as the carrier gas with flow rate $0.952\ L \cdot min^{-1}$. Each sample was measured for three times or more, and the average value was reported. Some selected samples were also characterized by UV–vis spectrometer (UV-2450, Shimadzu Corporation) with 5 nm slit width. The solid phase was characterized by X-ray diffraction (XRD, D8-Advance, 40 kV, 40 mA) using Cu K_α radiation at a $5°\ min^{-1}$ scanning rate.

3. Results and Discussion

3.1. Solubility of $FePO_4 \cdot 2H_2O$ in deionized water

The solubility data of $FePO_4 \cdot 2H_2O$ in deionized water (18.2 MΩ) at temperatures from 298.15 to 363.15 K and atmosphere pressure are presented in Table 2. Herein, we assume that $FePO_4 \cdot 2H_2O$ dissociates to Fe^{3+} and PO_4^{3-}, and the solubility product (K_{sp}) of $FePO_4 \cdot 2H_2O$ is expressed as Eq. (1).

$$K_{sp} = \left[Fe^{3+}\right] \times \left[PO_4{}^{3-}\right] \times [H_2O]^2 \quad (1)$$

Table 2
Solubility of $FePO_4 \cdot 2H_2O$ in deionized water at 298.15 to 363.15 K and atmospheric pressure①

T/K	$FePO_4 \cdot 2H_2O$ solubility $\times 10^6$ /g·kg^{-1}	Appearance of residues	T/K	$FePO_4 \cdot 2H_2O$ solubility $\times 10^6$ /g·kg^{-1}	Appearance of residues
298.15	1.48 + 0.05	Light yellow	323.15	1.20 ± 0.02	Light yellow
303.15	1.45 ± 0.04	Light yellow	333.15	1.04 ± 0.02	Light yellow
308.15	1.40 ± 0.03	Light yellow	343.15	0.72 ± 0.02	Light yellow
313.15	1.37 ± 0.03	Light yellow	353.15	0.58 ± 0.01	Light yellow
318.15	1.27 ± 0.02	Light yellow	363.15	0.11 ± 0.004	Light yellow

① The standard uncertainty of the temperature is 0.1 K; standard uncertainty of the pressure is 0.005 MPa; the relative standard uncertainty for concentration of $FePO_4 \cdot 2H_2O$ is below 0.05.

In the aqueous solution, Fe^{3+} could be hydrolyzed to $Fe(OH)^{2+}$ and $Fe(OH)_2^+$; phosphoric acid has a three-step dissociation process generating various phosphate anions [29]. When using deionized water as solvent, the content of phosphorus equals to that of iron in solution; the interaction between iron species and phosphate species could be neglected because the concentration of OH^- is much higher than that of phosphate species. As the contents of phosphorous and iron in solution being measured, the concentrations of Fe^{3+} and PO_4^{3-} can be calculated according to the hydrolysis constant of Fe^{3+} and the dissociation constant of phosphoric acid previously reported [30,31] directly. In this work, the K_{sp} of $FePO_4 \cdot 2H_2O$ at 298.15 K was calculated as 5.39×10^{-29}, close to Dean's report (9.92×10^{-29}) [28]. It indicates the reliability of our solubility measurements. From Table 2, it could be found that the solubility of $FePO_4 \cdot 2H_2O$ monotonously decreases with the temperature increasing. The solubility at 343.15 K is only half of that at 298.15 K.

Table 1
The composition, pH value and density of various solvents

Entry	1	2	3	4	5	6	7	8	9	10
H_3PO_4 concentration/wt%	0.00	1.13	2.24	3.33	4.33	5.51	6.57	7.62	8.63	10.7
pH	7.02	1.35	1.13	0.98	0.90	0.82	0.75	0.69	0.64	0.52
ρ/g·ml^{-1}	1.015	1.022	1.027	1.034	1.038	1.042	1.050	1.055	1.065	1.072

3.2. Solubility of $FePO_4 \cdot 2H_2O$ in various H_3PO_4 solutions

The dissolution behavior of $FePO_4 \cdot 2H_2O$ in H_3PO_4 solutions is complex due to the formation of various complex ions at acidic environment. The composition of complex ion is significantly dependent on the amount of H_3PO_4 acid. Considering the interactions between one iron ion and one phosphate ion only, Stumm *et al.* indicated that $FeHPO_4^+$ was of majority when the concentration of H^+ was below 2×10^{-2} mol·L^{-1}, otherwise $FeH_2PO_4^{2+}$ was the main species [32]. While, when the concentration of H_3PO_4 was largely excessive over that of iron ions, multi-ligands complex may become dominant, such as $Fe(H_2PO_4)^{2+}$, $FeH_3(PO_4)_2$, $FeH_5(PO_4)_2^{2+}$, $Fe(H_2PO_4)_3$, and $FeH_7(PO_4)_3^+$ [33]. The $FePO_4 \cdot 2H_2O$ crystals with varied morphologies and structures were usually synthesized under such conditions, but until now, little thermodynamic knowledge is available about these complexes, and there is no report on the solubility data of $FePO_4 \cdot 2H_2O$ at high H_3PO_4 concentration (≥0.1 mol·L^{-1}). Herein, we measured the solubility of $FePO_4 \cdot 2H_2O$ in H_3PO_4 solutions with its concentration from 1.13 wt% to 10.7 wt% and temperatures from 298.15 to 363.15 K. All the results are listed in Table 3.

As seen, the solubility of $FePO_4 \cdot 2H_2O$ in 1.13 wt% H_3PO_4 is 0.490 g·kg^{-1} at 298.15 K, even more than three hundred thousand times of that in deionized water (1.48×10^{-6} g·kg^{-1}). The jump of solubility with H_3PO_4 addition implies that some complex interactions between Fe^{3+} and phosphate ions become significant to convert Fe^{3+} to soluble coordination species, and boost the dissolving of $FePO_4 \cdot 2H_2O$. In detail, $H_2PO_4^-$ is of the main anionic species in the solution containing 1.13 wt% H_3PO_4, so the iron in the soluble $(FeH_2PO_4)^{2-}$ can be much more than that as Fe^{3+} and results in abnormal growth of solubility. When the H_3PO_4 concentration increases from 1.13 wt% to 10.7 wt%, the solubility of $FePO_4 \cdot 2H_2O$ increases further, but the trend becomes smooth. Fig. 1 shows the phenomena intuitively, in which the variance of the solubility of $FePO_4 \cdot 2H_2O$ could reach one to two orders of magnitude. We attempt to calibrate the solubility of $FePO_4 \cdot 2H_2O$ (y) with the H_3PO_4 concentration (x) by equation $y = A \cdot x^b$. Table 4 lists the calibration results. At every temperature except for 298.15 K, the correlation coefficients are over 0.95, indicating that the calibration results agree with the measurements well. The exponent b determines the sensitivity of the solubility of $FePO_4 \cdot 2H_2O$ on the H_3PO_4 concentration. As the temperature is 308.15 K or higher, b almost keeps in the range from 2.4 to 2.8. In other words, doubling the H_3PO_4 concentration could increase the solubility of $FePO_4 \cdot 2H_2O$ by 5 to 7 times. As for the effect of temperature on the solubility of $FePO_4 \cdot 2H_2O$, the case of using H_3PO_4 solution as solvent is similar with that of using deionization water as solvent, *i.e.*, the solubility of $FePO_4 \cdot 2H_2O$ decreases with the increasing of

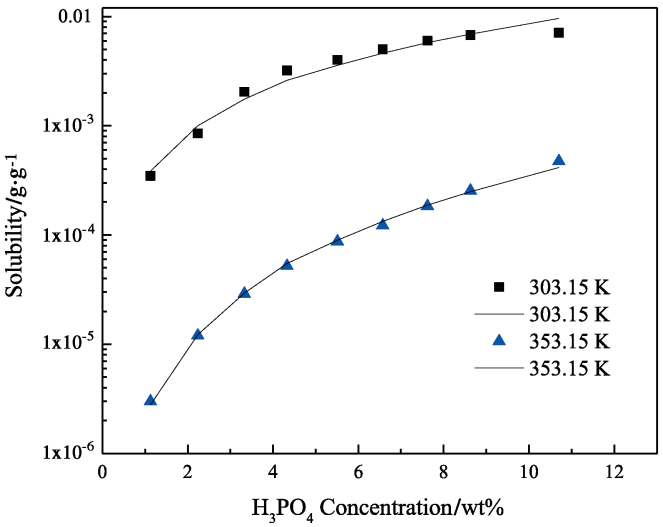

Fig. 1. The dependence of solubility of $FePO_4 \cdot 2H_2O$ on the concentration of H_3PO_4 at atmospheric pressure. The dots and lines correspond to the experimental data and calculated results, respectively.

Table 4
Parameters for calibrating the solubility of $FePO_4 \cdot 2H_2O$ with H_3PO_4 concentration

T	A	b	r^2	T	A	b	r^2
298.15	0.0325	0.612	0.721	323.15	0.353	2.68	0.998
303.15	0.0827	1.05	0.958	333.15	0.377	2.76	0.996
308.15	1.57	2.43	0.952	343.15	0.129	2.42	0.983
313.15	7.07	3.39	0.994	353.15	0.189	2.68	0.997
318.15	0.589	2.74	0.981	363.15	0.206	2.76	0.991

Table 3
Solubility of $FePO_4 \cdot 2H_2O$ in various concentrations of H_3PO_4 solutions at 298.15 to 363.15 K and atmospheric pressure①

H_3PO_4concentration /g $H_3PO_4 \cdot (100\ g\ H_2O)^{-1}$	$FePO_4 \cdot 2H_2O$ solubility /g·kg^{-1}					Appearance of residues
	298.15 K	303.15 K	308.15 K	313.15 K	318.15 K	
1.13	0.490 ± 0.006	0.346 ± 0.004	0.022 ± 0.000	0.015 ± 0.000	0.008 ± 0.000	White
2.24	1.268 ± 0.011	0.851 ± 0.007	0.126 ± 0.001	0.050 ± 0.001	0.025 ± 0.000	White
3.33	5.658 ± 0.082	2.038 ± 0.021	0.282 ± 0.002	0.182 ± 0.002	0.105 ± 0.001	White
4.33	6.170 ± 0.095	3.196 ± 0.030	0.503 ± 0.004	0.341 ± 0.002	0.189 ± 0.002	White
5.51	6.403 ± 0.103	4.006 ± 0.043	0.808 ± 0.006	0.417 ± 0.004	0.229 ± 0.002	White
6.57	6.523 ± 0.105	5.012 ± 0.060	1.570 ± 0.013	0.589 ± 0.004	0.307 ± 0.002	White
7.62	6.666 ± 0.097	5.973 ± 0.052	3.960 ± 0.041	1.097 ± 0.007	0.561 ± 0.004	White
8.63	6.879 ± 0.101	6.760 ± 0.058	4.546 ± 0.034	1.750 ± 0.019	0.928 ± 0.004	White
10.7	7.398 ± 0.114	7.102 ± 0.086	6.566 ± 0.058	3.617 ± 0.034	1.956 ± 0.029	White
	323.15 K	333.15 K	343.15 K	353.15 K	363.15 K	
1.13	0.006 ± 0.000	0.005 ± 0.000	0.004 ± 0.000	0.003 ± 0.000	0.003 ± 0.000	White
2.24	0.021 ± 0.000	0.016 ± 0.000	0.013 ± 0.000	0.012 ± 0.000	0.011 ± 0.000	White
3.33	0.051 ± 0.001	0.036 ± 0.000	0.031 ± 0.000	0.029 ± 0.000	0.025 ± 0.000	White
4.33	0.103 ± 0.001	0.075 ± 0.001	0.054 ± 0.001	0.052 ± 0.001	0.050 ± 0.001	White
5.51	0.153 ± 0.002	0.123 ± 0.001	0.090 ± 0.002	0.087 ± 0.001	0.081 ± 0.001	White
6.57	0.252 ± 0.002	0.187 ± 0.002	0.159 ± 0.002	0.122 ± 0.001	0.119 ± 0.001	White
7.62	0.370 ± 0.004	0.300 ± 0.004	0.267 ± 0.002	0.184 ± 0.002	0.164 ± 0.001	White
8.63	0.626 ± 0.004	0.473 ± 0.007	0.398 ± 0.004	0.254 ± 0.002	0.215 ± 0.002	White
10.7	1.335 ± 0.006	0.946 ± 0.013	0.789 ± 0.004	0.474 ± 0.007	0.443 ± 0.006	White

① The standard uncertainty of the temperature is $u(T) = 0.1$ K; standard uncertainty of the pressure is $u(p) = 0.005$ MPa; the relative standard uncertainty for concentration of $FePO_4 \cdot 2H_2O$ is below $u(r) = 0.02$.

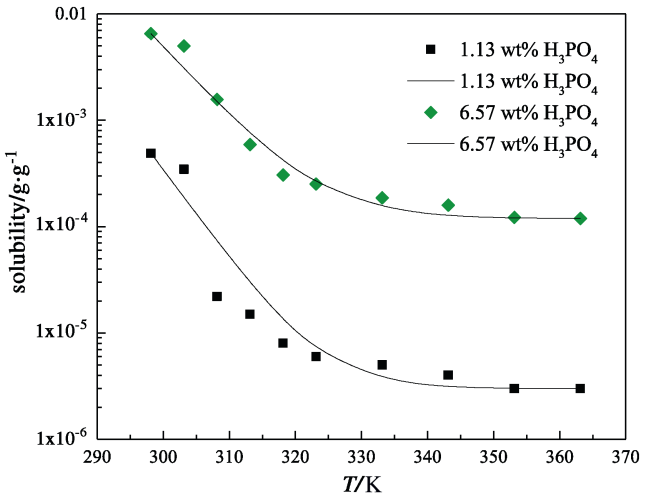

Fig. 2. The dependence of solubility of $FePO_4 \cdot 2H_2O$ on temperature at atmospheric pressure. The dots and lines correspond to the experimental data and calculated results, respectively.

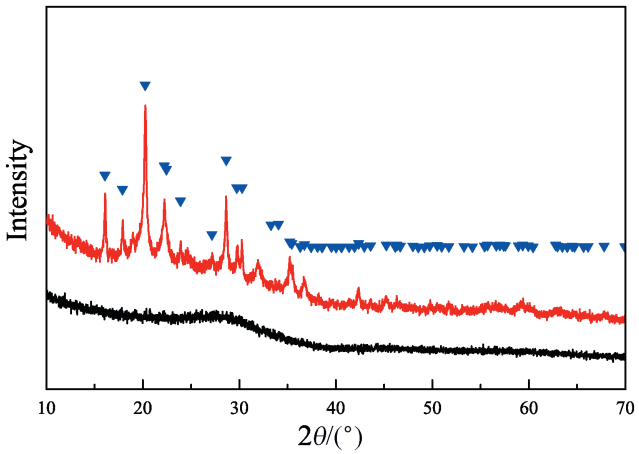

Fig. 3. XRD spectra of solid residues in water (bottom) and in 5.51 wt% H_3PO_4 solution (top) at 353.15 K.

temperature. Fig. 2 shows two typical curves reflecting the effect of temperature. The solubility seems to approach a constant value with the increasing of temperature, so we attempt to exploit equation $y = y_0 + A \cdot e^{-x/t}$ to calibrate the solubility (y) with temperature (x). Table 5 lists the calibration results. The correlation coefficients can reach 0.90 to 0.95. With the increasing of H_3PO_4 concentration, y_0 almost increases monotonously as expected, and t increases in general. The increasing of t implies that the sensitivity on temperature decreases. Considering the effects of temperature and H_3PO_4 concentration comprehensively, high temperature and low H_3PO_4 concentration are appropriate to enlarge the relative variance of solubility with temperature or H_3PO_4 concentration adulation. Otherwise, low temperature and high H_3PO_4 concentration should be selected to shrink the relative variance of solubility. The two groups of calibrating equations, with the H_3PO_4 concentration and temperature as independent variables, respectively, could be used to predict the solubility of $FePO_4 \cdot 2H_2O$ in H_3PO_4 solutions with concentration from 1.13 wt% to 10.7 wt% at temperatures from 298.15 K to 363.15 K.

3.3. The identification of the solid phase

It should be noticed that the solid residues have different appearances in Tables 1 and 2. In Table 1, the residues obtained in deionized water were light yellow, the same with the original amorphous $FePO_4 \cdot 2H_2O$. In Table 2, all the residues obtained in H_3PO_4 solutions turn to be white without exception. We used X-ray diffraction technique to check whether crystalline phase transition takes place in powder samples, Fig. 3 presents XRD patterns for two typical samples. One corresponds to the light yellow powders obtained in water at 353.15 K. The other corresponds to the white powders obtained in 5.51 wt% H_3PO_4 solution at 353.15 K. As seen, there is no diffraction peak detected for the light yellow powders, indicating the amorphous feature of residual $FePO_4 \cdot 2H_2O$, the same with the original. Differently, after long residence in H_3PO_4 solutions, the white powders obtained in 5.51 wt% H_3PO_4 addition at 353.15 K show sharp diffraction peaks in good agreement with orthorhombic $FePO_4 \cdot 2H_2O$ standard data of PDF no. 33-0667. The results evidence that the $FePO_4 \cdot 2H_2O$ in H_3PO_4 solutions experiences the dissolution of amorphous $FePO_4 \cdot 2H_2O$ and followed recrystallization of orthorhombic $FePO_4 \cdot 2H_2O$. Compared with the amorphous $FePO_4 \cdot 2H_2O$, the orthorhombic $FePO_4 \cdot 2H_2O$ is more stable in thermodynamics in aqueous solution. Since the transformation from amorphous $FePO_4 \cdot 2H_2O$ to orthorhombic $FePO_4 \cdot 2H_2O$ abides a dissolution–recrystallization mechanism, the solubility of amorphous $FePO_4 \cdot 2H_2O$ may determine the rate of the whole process. In water, the extremely low solubility of amorphous $FePO_4 \cdot 2H_2O$ leads that the transformation seems to be blocked during 30 days of experiment. *Vice versa*, the addition of H_3PO_4 makes the transformation process accelerates much and becomes remarkable.

3.4. Understanding iron phosphate materials preparation based on the solubility data

The soluble iron and phosphorus, determined by solubility in thermodynamics, is of iron source and phosphorus source for iron phosphate materials preparation. So, the information on the solubility and dissolving process of $FePO_4 \cdot 2H_2O$ can help to understand and design the preparation of various iron phosphate materials. In detail, for amorphous iron phosphate materials, the long residence of as prepared products in H_3PO_4 solution should be avoided to inhibit the crystalline phase transition, and high temperature is suitable to decrease the size of products by decreasing the solubility as well as increasing the supersaturation. For the preparation of iron phosphate crystalline materials by dissolution–recrystallization mechanism, high temperature and high H_3PO_4 concentration are appropriate conditions, since high H_3PO_4 concentration can improve the dissolution of precursors and high temperature can decrease the solubility of final products and increase the yield. When using $FePO_4 \cdot 2H_2O$ as the controlled iron or phosphorous

Table 5
Parameters for calibrating the solubility of $FePO_4 \cdot 2H_2O$ with temperature

	H_3PO_4 concentration/wt%								
Parameter	1.13	2.24	3.33	4.33	5.51	6.57	7.62	8.63	10.7
y_0	3.0×10^{-6}	1.1×10^{-5}	2.5×10^{-5}	5.0×10^{-5}	8.1×10^{-5}	1.2×10^{-4}	1.6×10^{-4}	2.2×10^{-4}	2.0×10^{-4}
A	4.6×10^{21}	1.3×10^{21}	9.3×10^{18}	4.8×10^{18}	6.6×10^{18}	5.3×10^{17}	5.6×10^{16}	3.1×10^{14}	1.1×10^{12}
t	5.19	5.39	6.10	6.21	6.16	6.50	6.94	7.89	9.28
r^2	0.902	0.934	0.990	0.975	0.958	0.938	0.957	0.965	0.912

sources, high H_3PO_4 concentration and low temperature could accelerate the providing of iron or phosphorous, while low H_3PO_4 concentration and high temperature have the opposite effect.

4. Conclusions

The solubilities of iron phosphate dihydrate in deionized water and phosphoric acid solutions at high mass concentrations from 1.13% to 10.7% were systematically measured at temperature from 298.15 to 363.15 K and atmosphere pressure. The solubility was found to increase 5 orders of magnitude or more with increasing the concentration of phosphoric acid, and decrease 1 to 2 orders of magnitude with increasing the equilibrium temperature. The phosphoric acid addition and temperature were found to affect the solubility of iron phosphate dihydrate by the formation or dissociation of coordination species, which could further accelerate the phase transformation from the amorphous iron phosphate dihydrate to orthorhombic iron phosphate dehydrate by dissolution–recrystallization mechanism. The high dependences of the solubility of iron phosphate materials on H_3PO_4 concentration and temperature could be well predicted by calibration equations and effectively exploited to regulate the precipitation, crystallization and growth processes between iron (III) and phosphate ions in aqueous solutions for synthesizing iron phosphate materials with diversified crystalline structure and morphology.

References

[1] Y.J. Lee, H. Yi, W. Kim, K. Kang, D.S. Yun, M.S. Strano, G. Ceder, A.M. Belcher, Fabricating genetically engineered high-power lithium-ion batteries using multiple virus genes, *Science* 324 (2009) 1051–1055.

[2] C.X. Guo, Y.Q. Shen, Z.L. Dong, X.D. Chen, W.X. Lou, C.M. Li, DNA-directed growth of $FePO_4$ nanostructures on carbon nanotubes to achieve nearly 100% theoretical capacity for lithium-ion batteries, *Energy Environ. Sci.* 5 (2012) 6919–6922.

[3] T.B. Zhang, Y.C. Lu, G.S. Luo, Synthesis of single-crystal dendrictic iron hydroxyl phosphste as s Fenton catalyst, *CrystEngComm* 15 (2013) 9104–9111.

[4] Y. Wang, X. Wang, Z. Su, Q. Guo, Q. Tang, Q. Zhang, H. Wan, SBA-15-supported iron phosphate catalyst for partial oxidation of methane to formaldehyde, *Catal. Today* 93–95 (2004) 155–161.

[5] D. Yu, J. Qian, N. Xue, D. Zhang, C. Wang, X. Guo, W. Ding, Y. Chen, Mesoporous nanotubes of iron phosphate: Synthesis, characterization, and catalytic property, *Langmuir* 23 (2007) 382–386.

[6] T.B. Zhang, Y.C. Lu, G.S. Luo, Iron phosphate prepared by coupling precipitation and aging: Morphology, crystal structure, and Cr (III) adsorption, *Cryst. Growth Des.* 13 (2013) 1099–1109.

[7] X.X. Zhang, S.S. Tang, M.L. Chen, J.H. Wang, Iron phosphate as a novel sorbent for selective adsorption of chromium (III) and chromium speciation with detection by ETAAS, *J. Anal. At. Spectrom.* 27 (2012) 466–472.

[8] S. Benmokhtar, H. Belmal, A.E. Jazouli, J.P. Chaminade, P. Gravereau, S. Pechev, J.C. Grenier, G. Villeneuve, D. Waal, Synthesis, structure, and physicochemical investigations of the new α $Cu_{0.50}TiO(PO_4)$ oxyphophate, *J. Solid State Chem.* 180 (2007) 772–779.

[9] Y.M. Lai, X.F. Liang, S.Y. Yang, J.X. Wang, L.H. Cao, B. Dai, Raman and FTIR spectra of iron phosphate glasses containing cerium, *J. Mol. Struct.* 992 (2011) 84–88.

[10] P. Moreau, D. Guyomard, J. Gaubicher, F. Boucher, Structure and stability of sodium intercalated phases in olivine $FePO_4$, *Chem. Mater.* 22 (2010) 4126–4128.

[11] Y. Yin, P. Wu, H. Zhang, C. Cai, Enhanced cathode performance of amorphous $FePO_4$ hollow nanospheres with tunable shell thickness in lithium ion batteries, *Electrochem. Commun.* 18 (2012) 1–3.

[12] Y. Song, P.Y. Zavalij, M. Suzuki, M.S. Whittingham, New iron (III) phosphate phases: Crystal structure and electrochemical and magnetic properties, *Inorg. Chem.* 41 (2002) 5778–5786.

[13] Y. Fang, L. Xiao, J. Qian, X. Ai, H. Yang, Y. Cao, Mesoporous amorphous $FePO_4$ nanospheres as high-performance cathode material for sodium-ion batteries, *Nano Lett.* 14 (2014) 3539–3543.

[14] M. Moradi, Z. Li, J. Qi, W. Xing, K. Xiang, Y.M. Chiang, A.M. Belcher, Improving the capacity of sodium ion battery using a vireo-templated nanostructured composite cathode, *Nano Lett.* 15 (2015) 2917–2921.

[15] V. Mathew, S. Kim, J. Kang, J. Gim, J. Song, J.P. Baboo, W. Park, D. Ahn, J. Han, L. Gu, Y. Wang, Y.S. Hu, Y.K. Sun, J. Kim, Amorphous iron phosphate: Potential host for various charge carrier ions, *NPG Asia Mater.* 6 (2014), e138.

[16] P. Nagaraju, C. Srilakshmi, N. Pasha, N. Lingaiah, I. Suryanarayana, P.S. Sai Prasad, Effect of P/Fe ratio on the structure and ammoxidation functionality of Fe–P–O catalysts, *Appl. Catal. A Gen.* 334 (2008) 10–19.

[17] Y.C. Lu, T.B. Zhang, Y. Liu, G.S. Luo, Preparation of $FePO_4$ nano-particles by coupling fast precipitation in membrane dispersion microreactor and hydrothermal treatment, *Chem. Eng. J.* 210 (2012) 18–25.

[18] S. Scaccia, M. Carewska, P.P. Prosini, Thermoanalytical study of iron (III) phosphate obtained by homogeneous precipitation from different media, *Thermochim. Acta* 413 (2004) 81–86.

[19] E. Pierri, E. Dalas, The precipitation of ferric phosphate on porous polymer, *Colloids Surf. A Physicochem. Eng. Asp.* 139 (1998) 335–340.

[20] E. Pierri, D. Tsamouras, E. Dalas, Ferric phosphate precipitation in aqueous media, *J. Cryst. Growth* 213 (2000) 93–98.

[21] M.L. Escoda, F. Torre, V. Salvadó, The formation of mixed ligand complexes of Fe (III) with phosphoric and citric acids in 0.5 M $NaNO_3$ aqueous solutions, *Polyhedron* 18 (1999) 3269–3274.

[22] T. Roncal-Herrero, J.D. Rodríguez-Blanco, L.G. Benning, E.H. Oelkers, Precipitation of iron and aluminum phosphates directly from aqueous solution as a function of temperature from 50 to 200 °C, *Cryst. Growth Des.* 9 (2009) 5197-5205.

[23] K. Kandori, T. Kuwae, T. Ishikawa, Control on size and adsorptive properties of spherical ferric phosphate particles, *J. Colloid Interface Sci.* 300 (2006) 225–331.

[24] T. Zhang, Y. Lu, G. Luo, Size adjustment of iron phosphate nanoparticles by using mixed acids, *Ind. Eng. Chem. Res.* 52 (2013) 6962–6968.

[25] S.C. Chang, M.L. Jackson, Solubility product of iron phosphate, *Soil Sci. Soc. Am. Proc.* 21 (1957) 265–268.

[26] E.P. Egan, Z.T. Wakefield, B.B. Luff, Low temperature heat capacity and heat of formation of crystalline and colloidal ferric phosphate dihydrate, 65 (1961) 1265–1270.

[27] J.O. Nriagu, Solubility equilibrium constant of strengite, *Am. J. Sci.* 272 (1972) 476–484.

[28] R.J. Xie, M.J. Gomez, Y.J. Xing, P.S. Klose, Fouling assessment in a municipal water reclamation reverse osmosis system as related to concentration factor, *J. Environ. Eng. Sci.* 3 (2004) 61–72.

[29] T. Zhang, Y. Lu, D. Xin, G. Luo, Direct precipitation for a continuous synthesis of nanoiron phosphate with high purity, *Ind. Eng. Chem. Res.* 53 (2014) 6723–6729.

[30] A. Stefansson, T.M. Seward, A spectrophotometric study of iron (III) hydrolysis in aqueous solution to 200 °C, *Chem. Geol.* 249 (2008) 630–645.

[31] R.E. Mesmer, C.F. Bases, Phosphoric acid dissociation equilibria in aqueous solutions to 300 °C, *J. Solut. Chem.* 3 (1974) 307–322.

[32] H. Galal-Gorchev, W. Stumm, The reaction of ferric iron with ortho-phosphate, *J. Inorg. Nucl. Chem.* 25 (1963) 567–574.

[33] M. Iuliano, L. Ciavatta, G.D. Tommaso, On the solubility constant of strengite, *Soil Chem.* 71 (2007) 1137–1140.